Applied Catalysis B: Environmental 96 (2010) 83–93

Contents lists available at ScienceDirect

Applied Catalysis B: Environmental

journal homepage: www.elsevier.com/locate/apcatb

Pd and Pt ions as highly active sites for the water–gas shift reaction over combustion synthesized zirconia and zirconia-modified ceria

Parag A. Deshpande [a], M.S. Hegde [b], Giridhar Madras [a,b,*]

[a] Department of Chemical Engineering, Indian Institute of Science, Bangalore 560012, India
[b] Solid State and Structural Chemistry Unit, Indian Institute of Science, Bangalore 560012, India

ARTICLE INFO

Article history:
Received 10 October 2009
Received in revised form 22 January 2010
Accepted 3 February 2010
Available online 10 February 2010

Keywords:
Heterogeneous catalysis
Solid solutions
Oxide ion vacancy
Redox mechanism
Surface processes
Acid–base pairs

ABSTRACT

Noble metal substituted ionic catalysts were synthesized by solution combustion technique. The compounds were characterized by X-ray diffraction, FT-Raman spectroscopy, and X-ray photoelectron spectroscopy. Zirconia supported compounds crystallized in tetragonal phase. The solid solutions of ceria with zirconia crystallized in fluorite structure. The noble metals were substituted in ionic form. The water–gas shift reaction was carried out over the catalysts. Negligible conversions were observed with unsubstituted compounds. The substitution of a noble metal ion was found to enhance the reaction rate. Equilibrium conversion was obtained below 250 °C in the presence of Pt ion substituted compounds. The formation of Bronsted acid–Bronsted base pairs was proposed to explain the activity of zirconia catalysts. The effect of oxide ion vacancies on the reactions over substituted ceria–zirconia solid solutions was established.

1. Introduction

Synthesis of solids for applications in catalysis should impart some important characteristics to the solids. Mechanical properties like surface area, porosity, thermal and mechanical stability and surface characteristics have been identified as important parameters influencing the catalyst performance [1]. Therefore, the development of methods of the synthesis, which can restrict the crystallite size to nanometer dimensions, is of interest. Nanocrystalline solids provide high surface area, high surface accessibility, and ease of regeneration in case of carbon deposition or coking. The nanoscale dimensions and the shapes of the solids have been reported to influence the catalyst performance. Si and Flytzani-Stephanopoulos [2] have shown high shape dependence of CO conversion over Au–CeO_2 for the water–gas shift reaction (WGS). Zhau et al. [3] have shown higher activity of CeO_2 nanoflowers as compared to nanocubes and nanopolyhedra for CO oxidation.

Several investigators have shown the morphological effects of the solids on the catalytic properties [4–5]. High thermal stability has been observed by Crepaldi et al. [6] for the three-way catalysis in case of nanocrystalline ceria–zirconia thin films, and by Wang et al. [7] for ceria nanopowders. Kleinlogel and Gauckler [8] have shown that nanosized solid solutions of ceria with gadolinium added with suitable transition metals show size dependent sintering behavior, which render them suitable for use as catalytic electrodes. Therefore, it is desirable to synthesize solids for catalytic application by methods which can limit the crystallite size to nanometer range and impart good catalytic properties. The solution combustion technique is one of such methods. With this technique, solids with high specific surface and crystallite size in nanometer range can be obtained [9–11]. In this study, we have synthesized noble metal substituted nanosized zirconia and ceria–zirconia solid solutions by solution combustion technique and have carried out WGS over these materials.

WGS has been studied on supported catalysts involving zirconia and ceria–zirconia by several investigators. ZrO_2 supported Pt and Au compounds have been reported to catalyze WGS [12–19]. According to Boaro et al. [13], ZrO_2 exhibits polymorphism. This phenomenon provides different sites for the catalysis and makes it a suitable support. Although ZrO_2 is not easily reducible by H_2, its reducibility can be enhanced by introduction of Pt [20]. Since WGS involves oxidation of CO to CO_2 it may involve the corresponding reduction of the support and it becomes desirable to have a reducible support material. The introduction of Pt in ZrO_2 enhances the reducibility of the support and, therefore, Pt substituted ZrO_2 is expected to act as a good catalytic material for the WGS reaction.

According to Tibiletti et al. [12], noble metals supported over pure oxides like ZrO_2 or CeO_2 show lower activity as compared to

* Corresponding author. Tel.: +91 80 2293 2321; fax: +91 80 2360 0683.
E-mail addresses: giridhar@chemeng.iisc.ernet.in, giridharmadras@gmail.com (G. Madras).

0926-3373/$ – see front matter © 2010 Elsevier B.V. All rights reserved.
doi:10.1016/j.apcatb.2010.02.004

the corresponding mixed oxides. ZrO_2 has a poor reducibility as compared to CeO_2. However, the reducibility of CeO_2 can be enhanced by the introduction of ZrO_2. This has been proved experimentally as well as by DFT calculations [21–23]. Therefore, much attention has been focused towards the use of mixed oxides and solid solutions of CeO_2–ZrO_2. Such oxides have shown high activity towards gas phase oxidation reactions [24–27].

The catalytic activity of the solids has been reported to be greatly influenced by the preparation method [13,18–19,28]. The properties like crystallinity, crystal size, and surface area are dependent on the method of preparation. The solution combustion method is a novel technique for the synthesis of nanocrystalline catalytic compounds. We have previously reported the catalytic activity of noble metal substituted CeO_2 for exhaust catalytic applications [11]. In this study, we show the activity of the catalysts for WGS. The use of noble metal ion substitution for Zr^{4+} and Ce^{4+} in ZrO_2 and CeO_2–ZrO_2 solid solutions for WGS is not reported in the literature. This study provides an insight into the mechanism of WGS on the basis of the catalyst structure and the various experimental observations.

2. Experimental

2.1. Chemicals and instruments

Zirconium nitrate ($Zr(NO_3)_4{\cdot}5H_2O$, Loba Chemie, India), ceric ammonium nitrate ($(NH_4)_2Ce(NO_3)_6$, Loba Chemie, India), palladium chloride ($PdCl_2$, Loba Chemie, India), tetraammine platinum (II) nitrate ($(NH_3)_4Pt(NO_3)_2$, Sigma–Aldrich, USA) and oxalyldihydrazide ($C_2H_6N_4O_2$, Alfa Aesar, India) were used for the synthesis of the compounds. CO (10.33% in N_2, Chemix Speciality Gases, Bangalore, India), and ultrahigh purity H_2, CO_2 and N_2 (all from Vinayaka Gases, Bangalore, India) were used for the catalytic reactions.

The powder X-ray diffraction patterns (XRD) were recorded on Phillips X'pert diffractometer using CuKα radiations. The scan rate and 2θ range were fixed at 0.067 °/min and 5–90°, respectively, for all the scans. The X-ray photoelectron spectra (XPS) were recorded on Thermo Fisher Scientific Multilab 2000 (England) instrument with AlKα radiations (1486.8 eV). The FT-Raman spectra were recorded on NXR-FT Raman module (Thermo Scientific, USA) equipped with Ge detector and Nd:YVO_4 laser. An online gas chromatograph (Nano HP-I, Mayura Analyticals Pvt. Ltd., Bangalore, India) was used for the analysis of the product gas mixture during the catalytic reactions.

2.2. Catalyst synthesis

The compounds were synthesized using the solution combustion technique. The technique involves the combustion of a salt of the support and a noble metal salt with a fuel in a solution. Zirconium nitrate, Pd or Pt salt and oxalyldihydrazide (as a fuel) were taken in a molar ratio of 0.98:0.02:1.96. The chemicals were mixed in a crystallizing dish. A small amount of water was added to make the solution. A few drops of nitric acid were added to obtain a clear solution. The solution was heated in a preheated muffle furnace at 350 °C. The solution underwent a spontaneous combustion to yield noble metal substituted zirconia that could be represented by the formula $Zr_{0.98}M_{0.02}O_2$ (M = Pd or Pt). For the synthesis of ceria–zirconia solid solutions, ceric ammonium nitrate, zirconium nitrate, Pd or Pt salt and oxalyldihydrazide were taken in a molar ratio of 0.83:0.15:0.02:2.4 and the combustion steps were repeated. The product obtained could be represented by the formula $Ce_{0.83}Zr_{0.15}M_{0.02}O_{2-\delta}$. The porous combustion products thus obtained were finely ground and heated at 500 °C for 24 h.

2.3. Catalytic reactions

WGS was carried out over the above synthesized catalysts. The reactions were carried out with 2% CO concentration (by volume). A total flow rate of 100 ml/min was maintained. This corresponded to a dry space velocity of 95,000 h^{-1}. The reaction was carried out in a quartz tube reactor of 4 mm i.d. The catalysts were made into granules of 150–300 μm and packed between ceramic wool. A thermocouple was used for measuring the bed temperature. The thermocouple was dipped in the catalyst bed. The reactors were heated from outside using an electric heater. The temperature was regulated using a PID controller. The reactant gas mixture was sent through flow controllers to maintain a dry gas flow rate of 100 ml/min. Water was pumped using an HPLC pump. A constant water flow of 0.1 ml/min was maintained. The line used for supplying water till the reactor was heated using an external heating tape. The temperature of the line was maintained at 150 °C using a temperature controller to keep the water in vapour phase and avoid its condensation. Idakiev et al. [19] have studied the influence of H_2O/CO ratio on CO conversion. It was found that at a given temperature, the increase in H_2O has an effect over the % CO conversion only at very small H_2O/CO ratio (<10). At higher H_2O concentrations, the conversions remain independent of H_2O concentration. Therefore, the kinetics of reaction becomes independent of H_2O concentration. However, with an increase in H_2O concentration, the equilibrium shifts towards the forward direction. Therefore, high H_2O concentrations were used. The water line was joined with the gas line and the lines were heated to avoid the condensation of water. The unreacted water was condensed using a condenser dipped in an ice cold water bath. The dry product gas mixture was sent to an online gas-chromatograph unit (HP-Nano *I*, Mayura Analyticals Pvt. Ltd., Bangalore, India). A single step separation of all the gases in the mixture was done using Hayesep-A and molecular sieve columns. Flame ionization detector and thermal conductivity detectors were used for detection of all the components of the gas mixture.

3. Results and discussion

3.1. Structural analysis

The crystal structure of the synthesized compounds was determined by XRD and was confirmed by FT-Raman spectroscopy. For finding the structural parameters, the XRD data were Rietveld refined using the FullProf suite program 1.0 [29]. The algorithm utilizing the non-linear least square fit was used to compare the observed peak intensities against the theoretically calculated intensities. The symbols in the figures show the experimental XRD data, the solid lines show the predicted XRD pattern. The difference between the actual and theoretical pattern is shown by the light line at the bottom. Fig. 1 shows the Rietveld refined XRD pattern of as prepared ZrO_2. The diffraction lines could be indexed to the tetragonal phase of zirconia. Fitting of the data to the tetragonal structure gave satisfactory values of the reliability data. Table 1 shows the cell parameters, crystallite size and the refinement reliability data for all the compounds. The fitting of the pattern to the monoclinic and the cubic structure gave poor fitting parameters. Small peaks around 28°, 29° and 32° were observed in the XRD of all the ZrO_2 compounds. Fig. 2 shows the extended XRD of ZrO_2 compounds in a small 2θ range of 27–33°. The characteristic monoclinic lines appear in this region. Diffraction lines at 28.5°, 29° and 31.5° (marked by asterisks) could be observed. This showed the crystallization of a small amount of ZrO_2 in monoclinic phase.

The XRD spectra of the compounds were recorded both before and after the reaction to observe the changes in the crystal

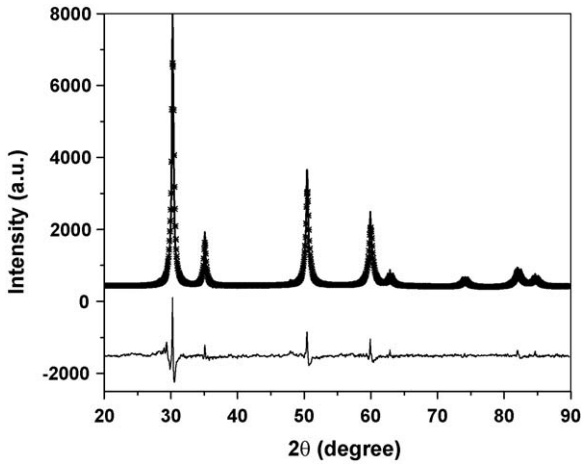

Fig. 1. Rietveld refined XRD pattern of ZrO_2.

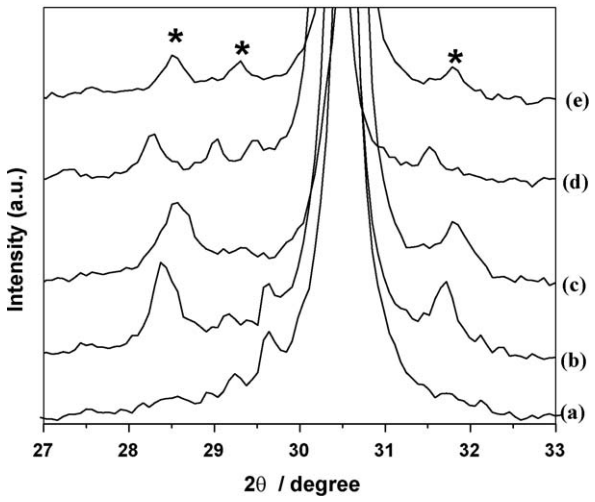

Fig. 2. Expanded XRD pattern of (a) ZrO_2, (b) $Pd_{0.02}Zr_{0.98}O_2$ before reaction, (c) $Pd_{0.02}Zr_{0.98}O_2$ after reaction, (d) $Pt_{0.02}Zr_{0.98}O_2$ before reaction and (e) $Pt_{0.02}Zr_{0.98}O_2$ after reaction showing monoclinic structure.

structure during the reaction. Fig. 3a and b show the Rietveld refined XRD pattern of Pd ion substituted ZrO_2 before and after the reaction. The parent tetragonal structure of the compound was retained. However, the reliability parameters for refinement of the compound after the reaction were inferior. The difference between the observed and calculated intensity near the first peak was high. This can be due to an increase in the monoclinic phase. For Pt substituted ZrO_2, the peak at 39° corresponding to Pt metal was observed in fresh as well as the used catalyst (Fig. 4a and b). This

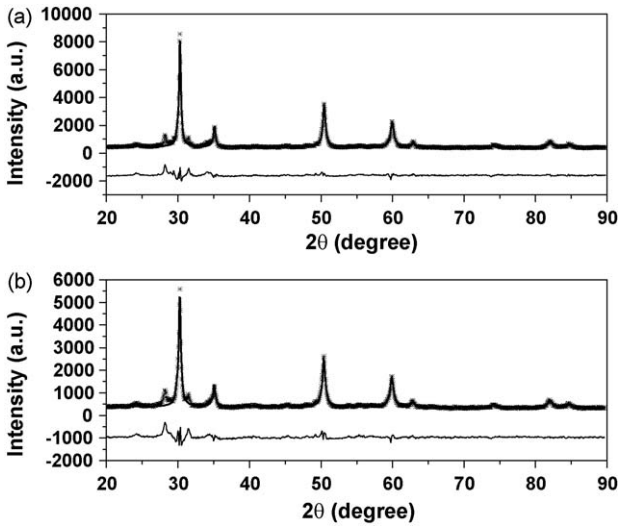

Fig. 3. Rietveld refined XRD pattern of $Pd_{0.02}Zr_{0.98}O_2$ (a) before reaction and (b) after reaction.

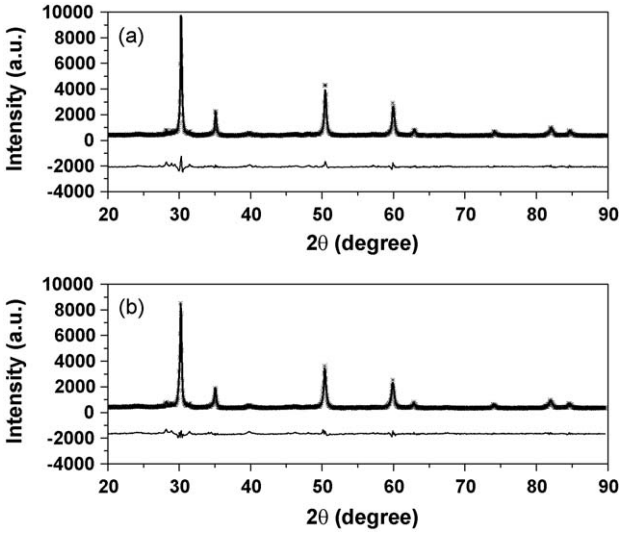

Fig. 4. Rietveld refined XRD pattern of $Pt_{0.02}Zr_{0.98}O_2$ (a) before reaction and (b) after reaction.

showed incomplete substitution of Pt in Zr^{4+} sites. However, the intensity of the peak was much lower than that obtained in case of the equivalent Pt impregnated ZrO_2 catalyst (see supporting information Fig. S1). Therefore, the majority of Pt was present as Pt ion that was substituted for Ce^{4+} ions in the lattice. XRD of Pt in

Table 1
Cell parameters for the different compounds obtained by Rietveld refinement.

Compound	Cell parameters (Å)			R_{Bragg}	R_F	$\chi 2$	Crystallite size (nm)
	a	*b*	*c*				
ZrO_2	3.6165(2)	3.6165(2)	5.1133(1)	5.22	2.45	5.34	31
$Zr_{0.98}Pd_{0.02}O_2$ (before reaction)	3.6197(2)	3.6197(2)	5.1110(1)	5.32	2.69	6.84	31
$Zr_{0.98}Pd_{0.02}O_2$ (after reaction)	3.6228(6)	3.6228(6)	5.1163(1)	7.15	3.17	7.42	31
$Zr_{0.98}Pt_{0.02}O_2$ (before reaction)	3.6182(6)	3.6182(6)	5.1125(3)	4.93	3.56	5.14	42
$Zr_{0.98}Pt_{0.02}O_2$ (after reaction)	3.6224(8)	3.6224(8)	5.1187(7)	5.47	5.29	6.13	31
$Ce_{0.85}Zr_{0.15}O_2$	5.3733(2)	5.3733(2)	5.3733(2)	4.08	3.42	5.03	18
$Ce_{0.83}Zr_{0.15}Pd_{0.02}O_{2-\delta}$ (before reaction)	5.3827(3)	5.3827(3)	5.3827(3)	6.12	4.11	7.47	25
$Ce_{0.83}Zr_{0.15}Pd_{0.02}O_{2-\delta}$ (after reaction)	5.3855(7)	5.3855(7)	5.3855(7)	5.63	3.82	6.29	33
$Ce_{0.83}Zr_{0.15}Pt_{0.02}O_{2-\delta}$ (before reaction)	5.3729(9)	5.3729(9)	5.3729(9)	6.56	4.77	7.89	24
$Ce_{0.83}Zr_{0.15}Pt_{0.02}O_{2-\delta}$ (after reaction)	5.3802(9)	5.3802(9)	5.3802(9)	6.27	4.54	7.5	25

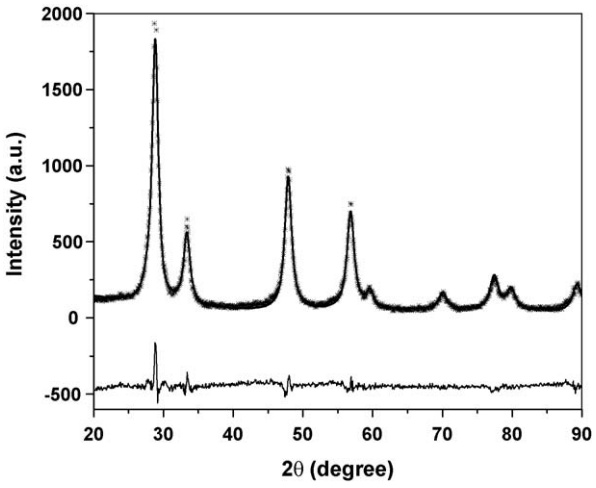

Fig. 5. Rietveld refined XRD pattern of $Ce_{0.85}Zr_{0.15}O_{2-\delta}$.

oxide form does not show any peak. Therefore, the peak at 39° in the XRD patterns of both substituted and impregnated catalysts correspond to the metal peak. The ratio of the metal peak intensity to the Zr(1 0 1) peak intensity in the different compounds gives the amount of Pt present in the compound in metallic form. The Pt/Zr(1 0 1) intensity in the impregnated compound was found to be 0.12 whereas it was 0.017 for the Pt ion substituted compound. Therefore, by comparing the intensity and attributing the intensity to the Pt metal, the amount of Pt metal in substituted compound was 14%. An increase in cell volume of $Zr_{0.98}Pt_{0.02}O_2$ by 0.35% was observed. This increase can be due to the formation of metallic Pd and Pt.

The XRD patterns of ceria–zirconia supported compounds were indexed to the fluorite structure of ceria with the space group *Fm*3*m*. Fig. 5 shows the Rietveld refined XRD pattern of $Ce_{0.85}Zr_{0.15}O_{2-\delta}$. It is to be noted here that all the lines in the pattern could be indexed exactly to the fluorite structure. No lines corresponding to tetragonal, monoclinic phase of zirconia were present. This showed complete substitution of Zr^{4+} in the lattice for Ce^{4+} ions. Fig. 6a and b show the Rietveld refined XRD of Pd ion substituted ceria–zirconia solid solution before and after the reaction. No diffraction line at 39° corresponding to Pd metal was observed in fresh as well as the used sample. Therefore, complete

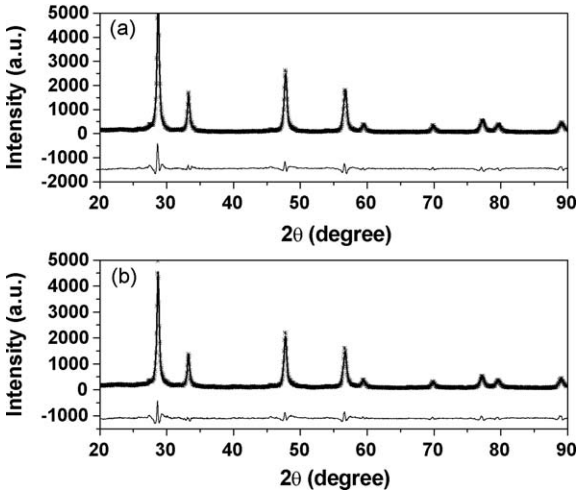

Fig. 6. Rietveld refined XRD pattern of $Pd_{0.02}Ce_{0.83}Zr_{0.83}O_{2-\delta}$ (a) before reaction and (b) after reaction.

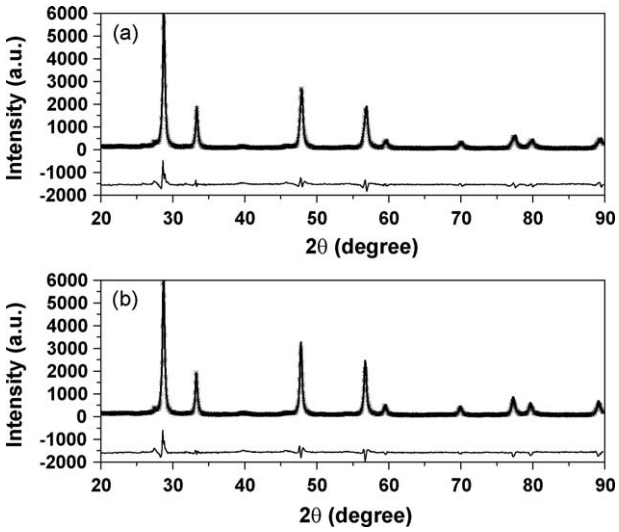

Fig. 7. Rietveld refined XRD pattern of $Pt_{0.02}Ce_{0.83}Zr_{0.83}O_{2-\delta}$ (a) before reaction and (b) after reaction.

substitution of Pd ions took place for Ce^{4+} ions and the compounds were solid solutions with formula $Ce_{0.83}Zr_{0.15}Pd_{0.02}O_{2-\delta}$. The metal ion remained in the lattice even after the reaction. No metal peak was observed in XRD after the reaction (Fig. 6b). The Rietveld refined XRD pattern of Pt ion substituted ceria–zirconia before and after the reaction is shown in Fig. 7a and b. A small peak at 39° was indeed observed in both the cases. No appreciable increase in the intensity of the peak was observed after the reaction, showing that the metal content did not change much after the reaction. To confirm the substitution of Pt in ionic state, XPS was recorded (discussed later), which showed nearly 75% ionic Pt substitution.

The presence of nanocrystals and wide XRD peaks make the distinction between the tetragonal and the cubic structure of ZrO_2 difficult exclusively on the basis of XRD information only [30]. To further confirm the crystal structure of the compounds, FT-Raman spectra were recorded. Fig. 8 shows the FT-Raman spectra of the as prepared compounds. The spectra for ZrO_2 in the Raman shift range of 100–700 cm^{-1} showed peaks mainly at 147, 265, 315, 459, 600 and 645 cm^{-1}, marked by asterisks. This is a characteristic of tetragonal phase of zirconia [31–32]. A single band at 490 cm^{-1} is the characteristic of cubic phase. In these compounds, no peak of

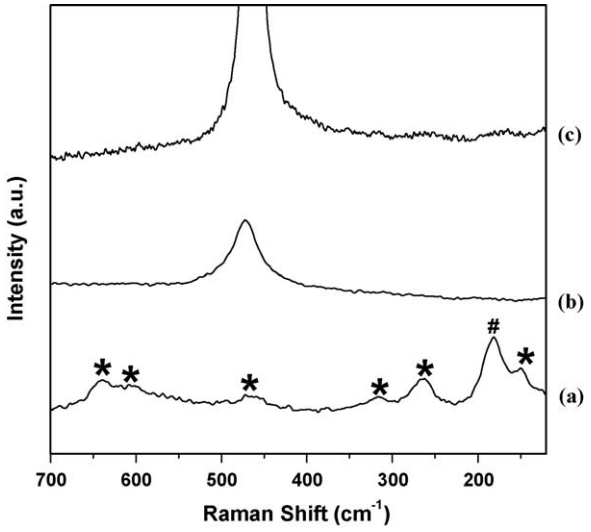

Fig. 8. FT-Raman spectra of as synthesized (I) ZrO_2, (II) $Ce_{0.85}Zr_{0.15}O_{2-\delta}$ and (III) CeO_2.

appreciable intensity was found near 490 cm^{-1}. This showed the crystallization of zirconia in a single phase tetragonal structure with a space group of $P4_2/mnc$. A small amount of monoclinic structure could also be detected from the peak at 180 cm^{-1} (marked #). The spectra of pure CeO_2 and $Ce_{0.85}Zr_{0.15}O_{2-\delta}$ are shown in Fig. 8b and c. A single peak at 465 cm^{-1} showed the presence of a single phase fluorite structure [33]. There were no signs of presence of any of the phases of zirconia.

All the peaks in the XRD were wide. This indicated the presence of crystallites in nanometer dimensions. The crystallite sizes of the compounds were calculated using the Scherrer formula and are given in Table 1. All the crystallites were found to be in the range of 20–40 nm. The crystallite size of $Ce_{0.85}Zr_{0.15}O_{2-\delta}$ was the smallest. However, the size increased after substitution. Small changes in the crystallite size were observed after the reaction but no trend could be established for the different compounds. The size remained unchanged for $Zr_{0.98}Pd_{0.02}O_2$ and $Ce_{0.83}Zr_{0.15}Pt_{0.02}O_{2-\delta}$ but it increased for $Ce_{0.83}Zr_{0.15}Pd_{0.02}O_{2-\delta}$ and decreased for $Zr_{0.98}Pt_{0.02}O_2$. But in all the cases, the size remained in nanometer dimensions and no bulk segregation of the particles was observed due to the imposed reaction conditions.

The oxidation states of the noble metals in the compounds were found using XPS. The spectra were recorded both before and after the reaction. After the experiment, the flow of the reactant gases was stopped and the catalysts were maintained at room temperature in a stream of N_2. To record the spectra of the spent catalyst, the catalyst was quickly transferred to the vacuum chamber of the spectrometer. To avoid the misleading spectra of the possible surface oxide species, the samples were etched in Ar stream. Different spent samples of the same catalyst obtained after different reaction runs were analyzed in the same manner and reproducible results were obtained. Fig. 9 shows the Pd3d spectra in $Zr_{0.98}Pd_{0.02}O_2$ and Fig. 10 shows Pd3d spectra in $Ce_{0.83}Zr_{0.15}Pd_{0.02}O_{2-\delta}$ before and after the reaction. The binding energies were calibrated with respect to the binding energy of graphite observed at 284.5 eV. The binding energies of Pd^0, Pd^{2+} and Pd^{4+} states are 335 and 340.6 eV, 337.5 and 342.9 eV, and 338.4 and 343.5 eV, respectively corresponding to the $3d_{5/2-3/2}$ spin-orbit doublet [34–36]. The binding energy of Zr2p also falls in the same range. Therefore, the spectra were decomposed to obtain the individual peaks corresponding to Pd3d and Zr2p. From the decomposed spectra of the fresh compounds (Figs. 9a and 10a), Pd was found to be substituted in +2 state in both the supports. This showed the ionic substitution of Pd in the lattice. The spectra were recorded after the reaction. In $Zr_{0.98}Pd_{0.02}O_2$, Pd remained in +2 state. However, Pd in metallic form was observed in case of $Ce_{0.83}Pd_{0.02}Zr_{0.15}O_{2-\delta}$.

The XPS of Pt4f in $Zr_{0.98}Pt_{0.02}O_2$, recorded before and after the reaction, is shown in Fig. 11a and b. The spectra obtained were very wide. The presence of wide peaks spanning binding energy more than 10 eV clearly showed the presence of multiple oxidation state. The spectra having non-zero intensities from 68 to 80 eV showed the presence of Pt^0, Pt^{2+} and Pt^{4+} states. For each oxidation state, two peaks corresponding to $Pt4f_{7/2-5/2}$ having an intensity ratio of 4:3 should be present. These peaks were approximated as the standard Gaussian peaks. The position, full width at half maxima and relative intensities of $Pt4f_{7/2}$–$Pt4f_{5/2}$ were fixed. The peak positions corresponding to the different oxidation states of Pt were found from literature [37–39]. The intensities ratio of peaks corresponding to $Pt4f_{7/2}$–$Pt4f_{5/2}$ was fixed at 4:3. The intensities of the different peaks were varied such that the root mean squared error of the resultant intensity was minimum.The peaks with maxima near 71.0 and 74.2 eV, 72.0 and 75.2 eV, and 74.4 and 77.6 eV were assigned to Pt^0, Pt^{2+} and Pt^{4+}, respectively [37–39]. Nearly 87% of the Pt was found to be in ionic state with very less metal in the fresh substituted zirconia. This value is in agreement with the XRD data, which

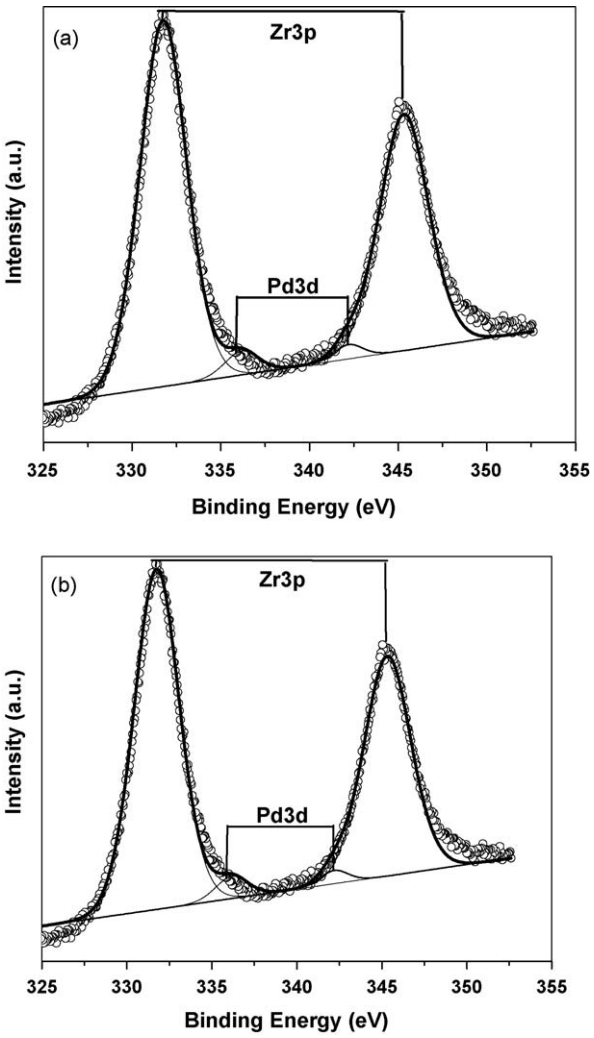

Fig. 9. Core level XPS of Pd3d in $Pd_{0.02}Zr_{0.98}O_2$ (a) before reaction and (b) after reaction.

showed 86% ionic substitution. Similarly, from the decomposed Pt4f spectra of $Ce_{0.83}Zr_{0.15}Pt_{0.02}O_{2-\delta}$ (Fig. 12a and b) nearly 76% of Pt was found to be in the ionic state in fresh catalysts. A weak XRD signal in Fig. 7 corresponds to the unsubstituted metal content. But, most of the Pt remains in ionic state. The spectra recorded after the reaction showed large changes in the oxidation states of Pt. For $Zr_{0.98}Pt_{0.02}O_{2-\delta}$, a large peak at 70.7 eV was observed after the reaction showing the formation of metallic Pt. A large decrease in Pt^{4+} state was observed (shown by peak at 74 eV). The change in Pt^{2+} state (shown by a peak at 72 eV) was negligible. Similarly, an increase in metal content was observed for $Ce_{0.83}Zr_{0.15}Pt_{0.02}O_{2-\delta}$, with a decrease in +4 state. However this decrease in Pt^{4+} was much lesser than that in $Zr_{0.98}Pt_{0.02}O_2$. Table 2 shows the changes in oxidation state of Pt for the two supports before and after the reaction. The XPS of Pt4f before and after the reaction for

Table 2
Percentage change in the oxidation state of Pt in the compounds before and after the reaction.

Compound		Pt^0	Pt^{2+}	Pt^{4+}
$Pt_{0.02}Zr_{0.98}O_2$	Before reaction	13	31	56
	After reaction	44	32	24
$Pt_{0.02}Ce_{0.83}Zr_{0.15}O_{2-\delta}$	Before reaction	24	47	29
	After reaction	34	78	10

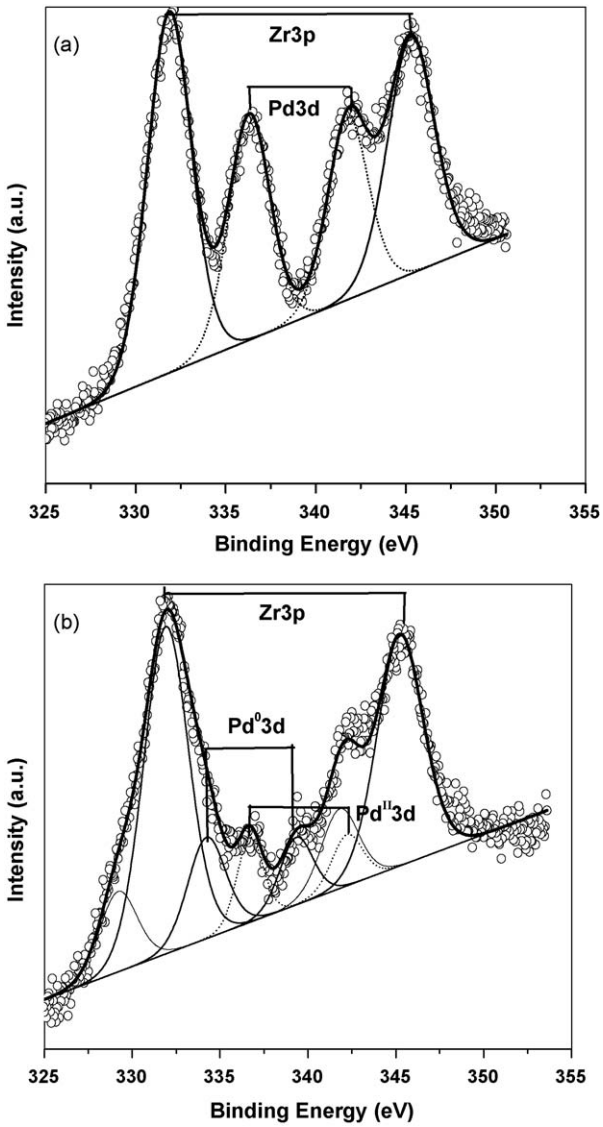

Fig. 10. Core level XPS of Pd3d in $Pd_{0.02}Ce_{0.83}Zr_{0.15}O_{2-\delta}$ (a) before reaction and (b) after reaction.

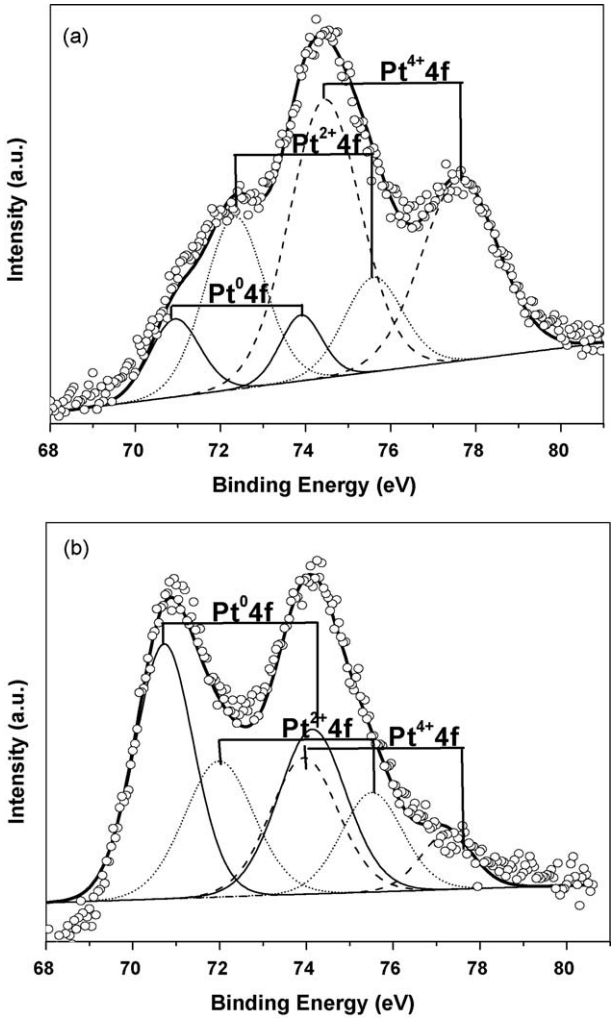

Fig. 11. Core level XPS of Pt4f in $Pt_{0.02}Zr_{0.98}O_2$ (a) before reaction and (b) after reaction.

impregnated Pt/ZrO_2 catalyst is shown in Fig. S2 (see supporting information). The intense peak at 71 eV shows the presence of Pt in metallic state. This shows that Pt was substituted in ionic form in combustion synthesized compounds, and Pt was in metallic form in impregnated compounds.

Fig. 13a and b show the Zr3d spectra. Zr was present in +4 state in all the compounds. For substituted ZrO_2, a small shift towards lower binding energy was observed after the reaction (Fig. 13a). This could be due to the formation of a small amount of Zr in +3 state. But the shift was lesser than 1 eV. Thus, Zr was present mainly in +4 state [40] and was not appreciably reduced. No reduction of Zr^{4+} was found in case of $Ce_{0.83}Zr_{0.15}M_{0.02}O_{2-\delta}$ compounds. Fig. 13c shows the Ce3d spectra in $Ce_{0.83}Zr_{0.15}M_{0.02}O_{2-\delta}$ compounds. In $Ce_{0.85}Zr_{0.15}O_{2-\delta}$ and in fresh $Ce_{0.83}Zr_{0.15}M_{0.02}O_{2-\delta}$ compounds, Ce was found to be present in +4 state. However, the partially filled valley can be seen in Figs. 13b and d showing the formation of Ce3+ in small amounts. Therefore, there was a reduction of Ce^{4+} to Ce^{3+} during the reaction.

3.2. Catalytic reactions

Fig. 14 shows the conversion of CO with temperature over the different catalysts. Pt ions showed higher activity as compared to the Pd ions over both the supports. With Pt substituted compounds, highest conversions could be obtained within 250–275 °C. Pd substituted compounds gave maximum conversion only above 325 °C. At temperatures above this temperature, a decrease in conversion was observed due to the reversible nature of the reaction.

In an industrial reformer, the outlet gas has a mixture of CO, CO_2, H_2 and several other hydrocarbons. Therefore, it is necessary to test the performance of the catalysts in the presence of CO_2 and H_2. WGS was carried out with a feed gas composition of 2% CO, 10% CO_2, 40% H_2, balanced with N_2 (all volume %) to make a total flow of 100 ml/min. Water was supplied at 0.1 ml/min. The conversion of CO over the different catalysts is shown in Fig. 15. The dotted lines show the equilibrium conversion. Equilibrium conversions as a function of temperature were calculated expressing the equilibrium in terms of the fugacity coefficients of the reactants and the products. The fugacity coefficients were determined using the generalized fugacity coefficient chart for gases and liquids [41].

The relation between the standard Gibbs free energy and the equilibrium constant is given as [41]

$$\Delta G - \Delta G^0 = RT \ln\left(\frac{\pi a_p^{\nu_p}}{\pi a_r^{\nu_r}}\right) \quad (1)$$

where ΔG the Gibbs free energy, ΔG^0 is the standard Gibbs free energy and T is the absolute temperature. a_p and a_r show the

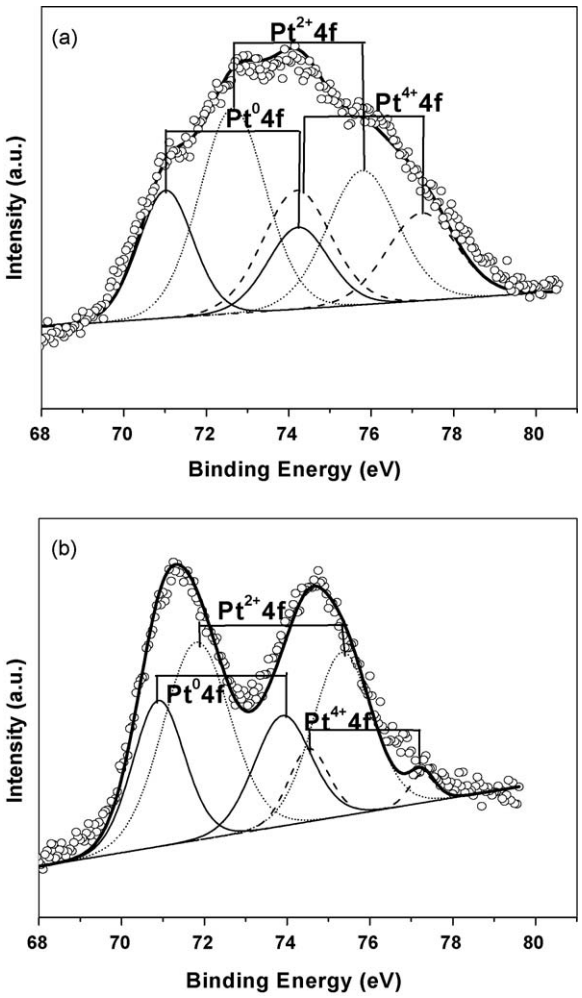

Fig. 12. Core level XPS of Pt4f in $Pt_{0.02}Ce_{0.83}Zr_{0.15}O_{2-\delta}$ (a) before reaction and (b) after reaction.

product and reactant species respectively with ν_i as the respective stoichiometry coefficient. At equilibrium,

$$K_a = \exp\left(\frac{-\Delta G^0}{RT}\right) \tag{2}$$

Expressing K_a in terms of the fugacity coefficients,

$$K_a = \left(\frac{\pi a_p^{\nu_p}}{\pi a_r^{\nu_r}}\right)\left(\frac{\pi (f/P)_p^{\nu_p}}{\pi (f/P)_r^{\nu_r}}\right) P^{\Delta \nu_i} \tag{3}$$

An expression giving the mole fraction as a function of temperature was obtained using Eqs. (2) and (3). A decrease in equilibrium conversion with temperature was obtained by solving the non-linear equation relating the conversion and the absolute temperature and a decreasing trend as shown in Fig. 15 was obtained which is a characteristic of exothermic reactions. Fig. 15a and b show the conversions obtained over Pt substituted compounds. Equilibrium conversions could be obtained only with these compounds. Pt substituted ZrO_2 was found to be the best catalyst with equilibrium conversion being attained below 250 °C. The rates of reaction were low as compared to those without H_2 and CO_2. This showed the effect of products in the feed gas. Due to the reversibility, the rates of reaction decreased with the introduction of products in the feed.

The Pd substituted compounds were affected by the presence of products in the feed (Fig. 15c and d). The maximum conversion was

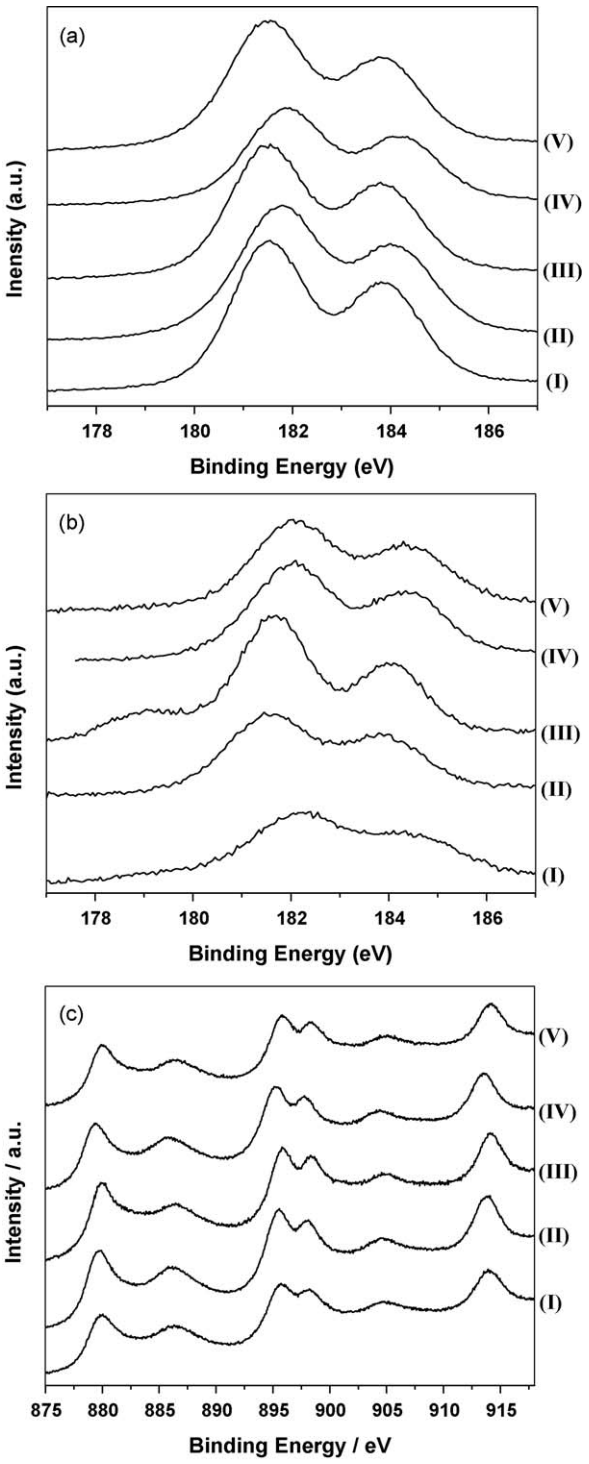

Fig. 13. Core level XPS of Zr3d in (a) (I) ZrO_2, (II) $Pd_{0.02}Zr_{0.98}O_2$ before reaction, (III) $Pd_{0.02}Zr_{0.98}O_2$ after reaction, (IV) $Pt_{0.02}Zr_{0.98}O_2$ before reaction, (V) $Pt_{0.02}Zr_{0.98}O_2$ after reaction, (b) (I) $Ce_{0.85}Zr_{0.15}O_2$, (II) $Pd_{0.02}Ce_{0.83}Zr_{0.15}O_2$ before reaction, (III) $Pd_{0.02}Ce_{0.83}Zr_{0.15}O_2$ after reaction, (IV) $Pt_{0.02}Ce_{0.83}Zr_{0.15}O_2$ before reaction, (V) $Pt_{0.02}Ce_{0.83}Zr_{0.15}O_2$ after reaction and (c) core level XPS of Ce3d (I) $Ce_{0.85}Zr_{0.15}O_2$, (II) $Pd_{0.02}Ce_{0.83}Zr_{0.15}O_2$ before reaction, (III) $Pd_{0.02}Ce_{0.83}Zr_{0.15}O_2$ after reaction, (IV) $Pt_{0.02}Ce_{0.83}Zr_{0.15}O_2$ before reaction, (V) $Pt_{0.02}Ce_{0.83}Zr_{0.15}O_2$ after reaction.

limited to 65% with $Ce_{0.85}Zr_{0.15}O_2$ support. Equilibrium conversion was not observed in any of the cases. With 100 mg of the catalyst, Pt substituted compounds showed nearly 57% conversion whereas with Pd substituted compounds, not even 10% conversion was possible. However, the behavior of the metal was found to be dependent upon the identity of the support. Pt worked better over

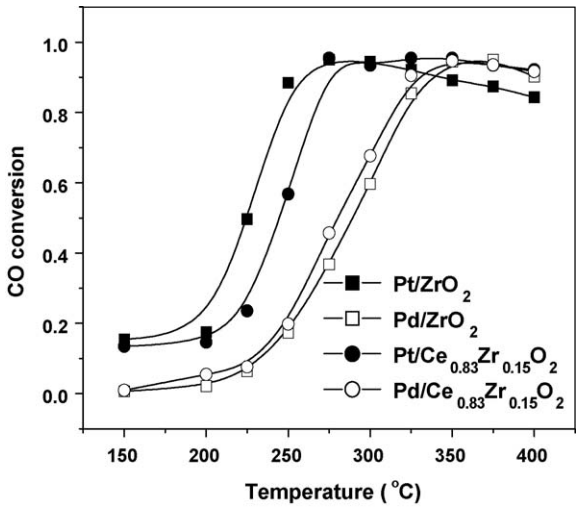

Fig. 14. Variation of CO conversion with temperature over the different catalysts in feed gas without CO_2 and H_2.

ZrO_2; Pd showed higher conversions over $Ce_{0.85}Zr_{0.15}O_2$ support. Therefore, there was indeed an involvement of support in catalyzing the reaction. Azzam et al. [42–43] discuss in detail the effect of support on the reaction sequence and the rates. Different activity of the same metal on the different supports was observed. Boaro et al. [13] have observed equilibrium conversions with ZrO_2 and CeO_2–ZrO_2 supported Au and Pt at temperatures above 350 °C. There have been reports of phase dependence of the rates for monoclinic and tetragonal ZrO_2 [15–16]. However, in all the cases, the equilibrium conversions were attained above 300 °C. Low temperature conversions have been reported by Idakiev et al. [19] while Tabakova et al. [18] have carried out WGS over ZrO_2 with Au and have found the equilibrium conversions being attained at temperatures as low as 240 °C. High activities were obtained with highly crystalline supports which included ZrO_2 and Fe_2O_3. However, they found that the activity was lower for mixed oxides. The lower activity was attributed to the inability of forming perfectly crystalline phases. We have previously reported the WGS activity of Pd and Pt ion substituted CeO_2 compounds [44]. It was found that the equilibrium conversions were possible only with Pt ion substitution. Further, no appreciable changes in the ionic state of the metal were observed after the reaction. This is in contrast to the current findings where we have observed Pt to get reduced to the metallic state after the reaction. Among all the catalysts tested, $Zr_{0.98}Pt_{0.02}O_2$ showed the highest activity towards WGS. The rates with Pd ion substitution were comparable for all the supports. Further, we have previously established the enhancement in the oxygen storage capacity and high rates of CO oxidation on using mixed oxide supports experimentally as well as by DFT calculations [21–22]. But contrary to our expectation, no appreciable increase in the rates was observed for the WGS with mixed oxide supports. Azzam et al. [43] have shown the support dependence of the rates for WGS and have found the rates to remain uninfluenced by using mixed supports. The rates with CeO_2 and $Ce_{0.85}Zr_{0.15}O_2$ supports were comparable for a given metal ion substitution. Pd substitution was found to be inferior to Pt substitution. The experiment carried out with impregnated Pt/ZrO_2 showed high initial activity (supporting information Fig. S3). But the rates were much lower at higher temperatures and equilibrium conversion could not be attained. The low activity of Pt metal impregnated ZrO_2 may be attributed to the poor dispersion of Pt metal in ZrO_2. Ionic dispersion of Pt in ZrO_2 results in high dispersion. Since XRD cannot capture very small metal particles and the irreducible nature of ZrO_2 results in the reduction of metal ion to metallic state, it is possible that all the phenomena taking place over ZrO_2 based catalysts are those involving Pt metal. Similarly, if a small amount of PtO is formed, the reduction of the same to Pt metal under the reducing conditions of the reaction can take place and the mechanism essentially becomes that over the metallic Pt. Therefore, for ZrO_2 based systems, the high dispersion of Pt is possible due to initial ionic dispersion. However, subsequent reduction to metallic form may take place, as can be seen from the XPS of Pt after the reaction.

The Pt-ion substituted compounds showed a light-off in the CO conversion curves, especially with higher catalyst weights (Fig. 15). The light-off was observed prominently for $Zr_{0.98}Pt_{0.02}O_2$.

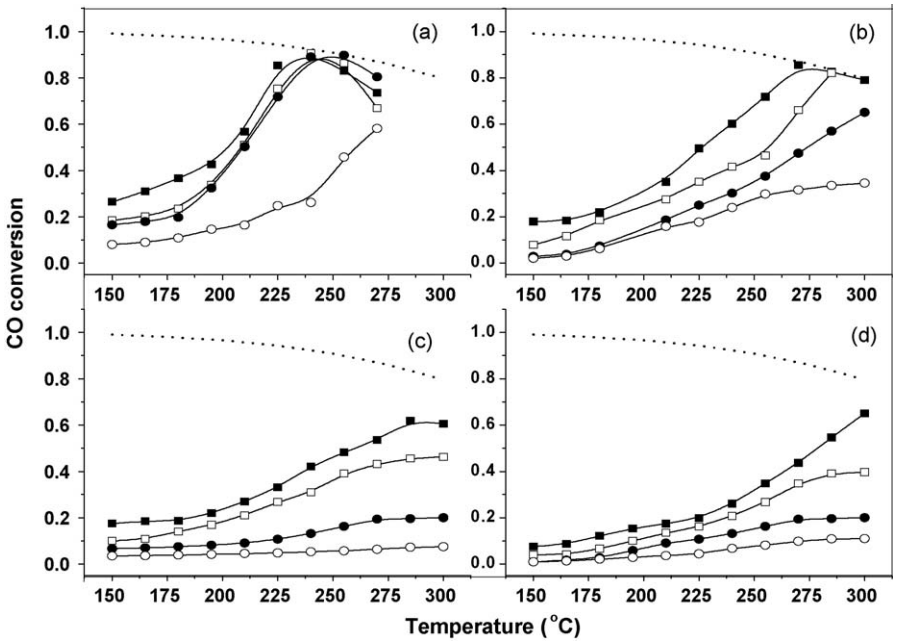

Fig. 15. Variation of CO conversion with temperature for the feed gas composition: CO = 2%, CO_2 = 10%, H_2 = 40%, balance N_2. (a) $Pt_{0.02}Zr_{0.98}O_{2-\delta}$, (b) $Pt_{0.02}Ce_{0.83}Zr_{0.15}O_2$, (c) $Pd_{0.02}Zr_{0.98}O_2$, (d) $Pd_{0.02}Ce_{0.83}Zr_{0.15}O_{2-\delta}$. Legends: (■) 500 mg, (□) 375 mg, (●) 250 mg, (○) 100 mg.

Also, the conversion was found to decrease above 250 °C. This type of behavior is shown by low temperature WGS catalysts [45]. Equilibrium conversions were attained at these temperatures. At higher temperatures, the reverse WGS reaction was observed, marked by a decrease in CO concentration with temperature.

To probe the reason behind the high activity of the compounds synthesized, we made use of the observations from XPS. For pure ceria, in the reducing atmosphere and at high temperatures, Ce^{3+} state is observed. With the generation of a small amount of Ce^{3+}, oxide ion vacancies are created in order to have an electrostatic balance [46].

$$4Ce^{4+} + O^{2-} \rightarrow (4Ce^{4+} + 2e^{-})/(\square + 0.5O_2) \rightarrow 2Ce^{4+} + 2Ce^{3+} + \square + 0.5O_2 \quad (4)$$

where □ shows the oxide ion vacancy created in the reduced ceria. From the XPS of as synthesized catalysts, both Pd and Pt were mainly in +2 state. This further induces the creation of oxide ion vacancies. For the charge balance, removal of one Ce^{4+} ion requires two Pt^{2+} or Pd^{2+} ions at the same site. Therefore, the oxide ion vacancies are created. These oxide ion vacancies play a vital role in catalysis. It should be noted that the above is not possible if the metals were impregnated in metallic form. Recently, Liu et al. [47] have reported the pathway for CO oxidation over ceria nanorods involving the oxide ion vacancy cluster. We have previously studied noble metal substituted ceria systems for CO oxidation and established the role of oxide ion vacancy [48–50]. The metal ion acts as the site for adsorption of CO. The exposure of the catalyst to CO results in the abstraction of oxygen from the intermediate oxygen species on the support. This is possible in reduced ceria only if there is a dissociative adsorption of oxygen on the support. Oxygen has very less adsorption over the bulk support. Therefore, the oxygen deficient oxide ion vacancies can be potential adsorption sites. A study by Martin and Duprez [51] has shown that an exchange of oxygen isotopes occurs between the support and the feed stream. This shows the high mobility of the oxygen in the support. Therefore, it is not merely the oxygen from the feed stream which reacts but oxidation occurs by the surface reaction of the adsorbed CO with the oxygen species in the support.

In case of WGS, there have been reports of surface activation by H_2O by oxide ion vacancies [52]. This step can be the possible step for the oxidation of the ceria for the completion of the catalytic cycle. The possible pathways for the reaction can be the direct dissociation of H_2O over the oxide ion vacancy, the formation of the intermediate oxygen species, and the surface reaction of the adsorbed CO and the oxygen species. Rodrigues et al. [53] have observed an increase in oxygen occupancy for Au/CeO_2 system signified by the changes in the lattice parameter after CO oxidation and WGS. A decrease in the lattice parameter with oxygen occupancy was observed. Ce^{4+} ion has a smaller size as compared to Ce^{3+} ion. Therefore, a decrease in oxygen occupancy showed transition from +4 to +3 state. Moreover, oxygen occupancy was found to decrease with the introduction of noble metal. This shows the effect of the noble metal in the creation of vacancy defects for charge balance. Therefore, $Ce^{4+} \leftrightarrow Ce^{3+}$ redox cycle is expected to take place over the ceria based catalysts (synthesized in this study) showing high activity.

In this study, ceria–zirconia solid solutions were prepared. The addition of Zr to CeO_2 resulted in the enhanced oxygen storage capacity. The experimental as well as the density functional theory calculations on CeO_2 and $Ce_{1-x}Zr_xO_2$ nanoparticles by Rodrigues et al. [53–54] showed enhanced oxygen storage capacity of Zr modified ceria. $Ce_{1-x}Zr_xO_2$ nanoparticles were found to have higher reducibility as compared to CeO_2 by H_2. Since WGS involves oxidation of CO to CO_2 and corresponding reduction of H_2O to H_2, it is always desirable to have a catalyst with high reducibility or oxygen storage capacity. The various oxygen atoms present in the solid solution are not all equivalent. The Zr–O bond distance in $Ce_{1-x}Zr_xO_2$ is greater than the normal Zr–O bond distance in ZrO_2 [21]. This results in creation of different oxygen species and as a result, the weakly bonded oxygen (one with greater bond length) is susceptible to be transferred for oxidation. The vacancy formation energy of $Ce_{1-x}Zr_xO_2$ is lesser than that of pure CeO_2 and results in higher reducibility [55–56]. Therefore, structurally Zr modified ceria is a better redox support as compared to CeO_2 alone. Although in this study, the rates were not greatly different from those over CeO_2 support, we had found large differences in the rate with Ti modified CeO_2 supports at very high H_2O supply [57].

The reducibility of the support and ionic nature of the metal played an important role in the reactions. We observed that the identity of the metal has an effect over the conversions. There have been experimental evidences of changing the redox properties of $Ce_{1-x}Zr_xO_2$ by the noble metal [58]. The metal–support interaction has been shown for $Ce_{1-x}Pt_xO_2$ system experimentally by electrochemical methods coupled with spectroscopic observations [59]. The redox cycles of Ce^{3+}–Ce^{4+} and Pt^{2+}–Pt^{4+} were observed as can be seen from the XPS of Pt4f (Fig. 12) and Ce3d (Fig. 13c). It was inferred that $Ce_{1-x}Pt_xO_2$ system reaches an equilibrium composition after evolution of the lattice oxygen. We have observed this phenomenon in the current study. Initially, a large decrease in CO concentration was observed without the stoichiometric formation of H_2 in spite of the continuous supply of H_2O. With time, the CO concentration was found to increase and when the reaction was allowed to take place at constant temperature for a long time, both CO and H_2 concentrations were found to become constant. This clearly indicates the utilization of lattice oxygen at the initial stages. The reduced $Ce_{1-x}Zr_xO_2$ support formed due to the loss of lattice oxygen is gradually regained by the oxidizing environment provided by splitting of H_2O.

In light of the above arguments, the following pathway can be proposed for WGS to take place over the noble metal substituted $Ce_{1-x}Zr_xO_2$.

$$Ce^{4+}_{1-x}Zr^{4+}_{x}O_2 \underset{-Ce^{4+}_{y}}{\overset{+M^{2+}_{y}}{\longrightarrow}} Ce^{4+}_{1-x-y}Zr^{4+}_{x}M^{2+}_{y}O_2 + y\square^{2+} \quad (5)$$

$$Ce_{1-x-y}Zr_xM_yO_2 + CO \overset{-((\delta-1)/2)O_2}{\longrightarrow} Ce_{1-x-y}Zr_xM_yO_{2-\delta} + CO_2 \quad (6)$$

$$Ce_{1-x-y}Zr_xM_yO_{2-\delta} + H_2O \overset{+((\delta-1)/2)O_2}{\longrightarrow} Ce_{1-x-y}Zr_xM_yO_2 + H_2 \quad (7)$$

The creation of oxide ion vacancy as a result of substitution of noble metal in +2 state for Ce^{4+} in order to have charge neutrality is shown in Eq. (5). The symbol □ shows the oxide ion vacancy. For the charge balance, the vacancy should have an equivalent +2 charge. The catalyst can undergo redox cycle in presence of an oxidizing or reducing environment. In WGS, CO provides a reducing environment. Therefore, the catalyst exists in reduced form. This is seen as removal of the lattice oxygen to make an oxygen deficient compound. The symbol δ signifies the donation of oxygen from the support rendering the catalyst to be in the reduced form. In presence of H_2O, the reduced form regains back its original form by abstracting oxygen from H_2O. Thus splitting of H_2O takes place over the reduced support. Thus, WGS takes place over the catalyst as a redox cycle, CO getting oxidized to CO_2 reducing the support and H_2O getting reduced to H_2 oxidizing the support. Therefore, the rate of reaction is dependent upon the nature of the support. The higher reducibility of the support results in higher rates of the redox cycle and hence higher rates of reaction. However, the enhancement in the reaction rates with introduction of Zr was not as high as those obtained for CO oxidation [21–23]. The possible reason behind this may be the weak oxidizing power of H_2O as compared to O_2 which was used for CO oxidation reactions. Bakhmutsky et al. [60] have

studied the effect of redox properties of the support for the WGS and have found that there is an optimum reducibility of the support at which the reaction rates are maximum. With highly reducible supports, excessive reduction of the support takes place which prevents further redox processes to take place. Boaro et al. [13] have also concluded that the bulk reducibility of the support plays only a secondary role. Therefore, although an increase is observed in the reaction rates with bulk Zr substitution, the effects are not very prominent at low H_2O supply rates.

As mentioned earlier, the metal–support interactions and changes in oxidation states of the metal and the support have been observed in noble metal substituted ceria systems [59]. The following equation can be written

$$Ce^{4+}_{1-x-y}Zr^{4+}_{x}M^{2+}_{y}O_2 + y\square^{2+} \leftrightarrow Ce^{3+}_{1-x-y}Zr^{4+}_{x}M^{4+}_{y}O_2 + \left(\frac{1-x-y}{2}\right)\square^{2+} \quad (8)$$

Ce^{3+}–Ce^{4+} cycles have been observed experimentally. Sharma and Hegde [59] have given an exhaustive treatment of the metal–support interaction and shown the Ce^{3+}–Ce^{4+} pairs spectroscopically in the similar compounds. Similarly, changes in Pt^{2+}–Pt^{4+} states were observed after the reaction. These show the presence of the cycle shown in Eq. (8). The creation of oxide ion vacancy due to change of Ce^{4+} to Ce^{3+} is well reported [45]. The above equation also shows a net increase in oxide ion vacancies. The value of y, the initial number of oxide ion vacancies, is lesser than the quantity $(1 - x - y)/2$ on the left hand side of the equation for small values of x and y. Therefore, substitution of zirconia as well as a noble metal resulted in the creation of more oxide ion vacancies favouring the redox cycle.

Therefore, on the basis of the above and the experimental observations, we propose the following phenomena to be taking place at the surface of the noble metal substituted $Ce_{1-x}Zr_xO_2$ solid solutions represented by Scheme 1.

The noble metal ion acts as an adsorption site for CO adsorption. CO adsorbed over the noble metal ion (M) is shown as CO_M. H_2O splits over the oxide ion vacancy to give an intermediate species 'O'. There have been spectroscopic evidences of the presence and stabilization of superoxide and peroxide species by CeO_2 [61]. The surface reaction between the adsorbed CO and 'O' results in the formation of the products.

The reducibility of ZrO_2 is lesser as compared to that of CeO_2. Still noble metal substituted ZrO_2 has shown high activity towards WGS. According to Miller and Grassian [62], the active sites include the Bronsted acid groups (OH groups), Lewis acids (Zr^{4+}), and the Lewis base sites (O^{2-}). The typical intermediates for reaction over Pt/ZrO_2 observed by Tibiletti et al. [12] include carbonyl and hydroxyl groups. In IR spectroscopic studies, Graf et al. [14] have proved the involvement of surface hydroxyl groups in the reaction. The structural modification of ZrO_2 by introduction of foreign

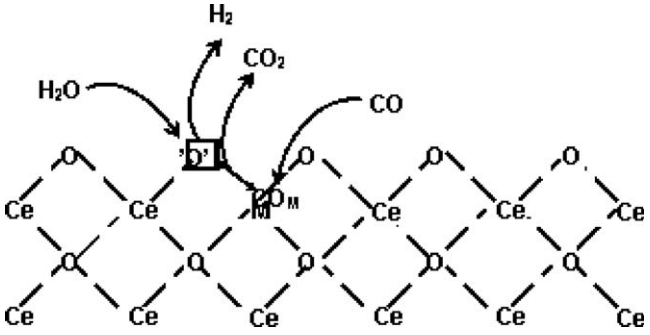

Scheme 1. Schematic illustration of the water–gas shift reaction over noble metal substituted ceria–zirconia solid solutions.

elements like Y has been reported to suppress the structural defects which are detrimental for the catalytic activity of the compound [63]. In their study, Zhu et al. [63] stabilized ZrO_2 using Y by replacing Zr^{4+} ions by Y^{3+} ions. The structural defects in the compound were found to be inactive for oxygen activation. However, in our catalysts, we use noble metal in ionic state and majority of Pt was in +4 state. Since the reducibility of Zr is much lower than that of Ce, Pt essentially remained in the metallic state as can be seen from the XPS of Pt4f after the reaction (Fig. 11b). Nearly 13% of Pt was present as metal in as prepared catalyst. But after the reaction, under the highly reducing environment of H_2 and CO, reduction of Pt 4+ state to metallic state took place. There was no change in the +2 state. From Table 2, it can be seen that the initial Pt^0:Pt^{2+}:Pt^{4+} ratio changed from 13:31:56 to 44:32:24 in the used catalyst. This clearly shows the reduction of Pt from +4 to zero state unlike $Ce_{1-x}Zr_xO_2$ supported Pt catalysts where large changes in both +2 and +4 states were observed. The initial composition of Pt^0:Pt^{2+}:Pt^{4+} = 24:47:29 changed to 24:78:10 after the reaction. The increase in +2 oxidation state and corresponding decrease in +4 state from the XPS support the redox mechanism involved in $CeZrO_2$ supports proposed by Eqs. ((5)–(7)) and Scheme 1. However, in case of ZrO_2 support, Pt in metallic form adsorbs CO. Zr^{4+} sites act as Lewis acids. This facilitates the adsorption of H_2O over the support. The formation of Lewis acid–base pairs Zr^{4+}–O^{2-} has been reported using FT–IR. [13] In the catalysts synthesized in this study, the noble metal atoms act as these sites for adsorption of CO. The following pathway can be proposed for WGS over the ZrO_2 supported compounds on the basis of the above observations

$$CO + S_M \leftrightarrow CO_M \quad (9)$$

$$ZrO_2 + 2H_2O \leftrightarrow Zr(OH)_4 \leftrightarrow H_2ZrO_3 + H_2O \quad (10)$$

$$CO_M + H_2ZrO_3 \rightarrow ZrO_2 + CO_2 + H_2 + S_M \quad (11)$$

The adsorption of H_2O over acidic Zr^{4+} sites takes place. This may result into the formation of surface hydroxyl groups which may interact with CO adsorbed over the adjacent site to give the products. During the catalytic cycle, the oxidation state of Zr remains +4 and the oxidation state of the metal remains 0. This is consistent with the experimental spectroscopic observations.

4. Conclusions

In this study, noble metal substituted ZrO_2 and $Ce_{1-x}Zr_xO_2$ solid solutions were synthesized by solution combustion technique. ZrO_2 compounds were found to crystallize in tetragonal structure with a small percentage of monoclinic ZrO_2 while the $Ce_{1-x}Zr_xO_2$ compounds were found to have a single phase fluorite structure. The noble metals were found to be in ionic form. The compounds were tested for the catalytic activity for the water–gas shift reaction. All the compounds showed CO conversion with corresponding formation of H_2. Pt substituted ZrO_2 was found to be the best catalyst showing equilibrium conversions below 250 °C. Pt in $Ce_{1-x}Zr_xO_2$ also gave equilibrium conversion but at a slightly higher temperature. Pd substitution was inferior as compared to Pt substitution. A reaction mechanism based upon the creation of oxide ion vacancies and the adsorption of CO over the noble metal ion was proposed for WGS over ceria–zirconia solid solutions. Utilization of acidic Zr^{4+} for dissociation of H_2O over ZrO_2 supports was proposed for the reaction over ZrO_2 supports.

Acknowledgements

Authors gratefully acknowledge the Indian Council for Agricultural Research (ICAR), Government of India, for financial assis-

tance. G.M. is thankful to the Government of India for the Swarnajayanti Fellowship.

Appendix A. Supplementary data

Supplementary data associated with this article can be found, in the online version, at doi:10.1016/j.apcatb.2010.02.004.

References

[1] J.A. Dumesic, G.W. Huber, M. Boudart, in: G. Ertl, H. Knozinger, F. Schuth, J. Weitkamp (Eds.), Handbook of Heterogeneous Catalysis, vol. 1, Wiley-VCH, Weinheim, 2008, p. 3.
[2] R. Si, M. Flytzani-Stephenopoulos, Angew. Chem., Int. Ed. 47 (2008) 2884.
[3] H.P. Zhau, Y.W. Zhang, H.X. Mai, X. Sun, Q. Liu, W.G. Song, C.H. Yan, Chem. Eur. J. 14 (2008) 3380.
[4] Tana, M., Zhang, J. Li, H. Li, Y. Li, W. Shen, Catal. Today, doi:10.1016/j.cattod.2009.02.016.
[5] J. Kunming, Z. Huili, L. Wencui, J. Catal. 29 (2008) 1089.
[6] E.L. Crepaldi, G.J. de, A.A. Soler-Illia, A. Bouchara, D. Grosso, D. Durand, C. Sanchez, Angew. Chem., Int. Ed. 42 (2003) 347.
[7] F.Y. Wang, G.B. Jung, A. Su, S.H. Chen, X.A. Li, M. Duan, T.C. Chiang, Mater. Lett. 63 (2009) 952.
[8] C. Kleinlogel, L.J. Gauckler, Adv. Mater. 13 (2001) 1081.
[9] K.C. Patil, M.S. Hegde, T. Rattan, S.T. Aruna, Chemistry of Nanocrystalline Oxide Materials: Combustion Synthesis, Properties and Applications, World Scientific, Singapore, 2008, p. 56.
[10] S.T. Aruna, A.S. Mukasyan, Curr. Opin. Solid State Mater. Sci. 12 (2008) 44.
[11] M.S. Hegde, G. Madras, K.C. Patil, Acc. Chem. Res. 42 (2009) 704.
[12] D. Tibiletti, F.C. Meunier, A. Goguet, D. Reid, R. Burch, M. Boaro, M. Vicario, A. Trovarelli, J. Catal. 244 (2006) 183.
[13] M. Barao, M. Vicario, J. Llorca, C. de Leitenberg, G. Dolcetti, A. Trovarelli, Appl. Catal., B 88 (2009) 272.
[14] P.O. Graf, D.J.M. de Vlieger, B.L. Mojet, L. Lefferts, J. Catal. 262 (2009) 181.
[15] E. Chenu, G. Jacobs, A.C. Crawford, R.A. Keogh, P.M. Patterson, D.E. Sparks, B.H. Davis, Appl. Catal., B 59 (2005) 45.
[16] J. Li, J. Chen, W. Song, J. Liu, W. Shen, Appl. Catal., A 334 (2008) 321.
[17] F. Menegazzo, F. Pinna, M. Signoretto, V. Trevison, F. Boccuzzi, A. Chiorino, M. Manzoli, ChemSusChem 1 (2008) 320.
[18] T. Tabakova, V. Idakiev, D. Andreeva, I. Mitov, Appl. Catal., A 202 (2000) 91.
[19] V. Idakiev, T. Tabakova, A. Naydenov, Z.Y. Yuan, B.L. Su, Appl. Catal., B 63 (2006) 178.
[20] P.S. Querino, J.R.C. Bispo, M.C. Rangel, Catal. Today 107–108 (2005) 920.
[21] T. Baidya, G. Dutta, M.S. Hegde, U.V. Waghmare, Dalton Trans. 455 (2009) 455.
[22] G. Dutta, U.V. Waghmare, T. Baidya, M.S. Hegde, K.R. Priolkar, P.R. Sarode, Catal. Lett. 108 (2006) 165.
[23] M.B. Bellakki, C. Shivkumara, T. Baidya, A.S. Prakash, N.Y. Vasanthacharya, M.S. Hegde, Mater. Res. Bull. 43 (2008) 2658.
[24] M. Zhao, M. Shen, J. Wang, J. Catal. 248 (2007) 257.
[25] B.M. Reddy, P. Bharali, P. Saikia, S.E. Park, M.W.E. van der Berg, M. Muhler, W.J. Grunert, J. Phys. Chem. C 112 (2008) 11729.
[26] T. Masui, K. Nakano, T. Ozaki, G. Adachi, Z. Kang, L. Eyring, Chem. Mater. 13 (2001) 1834.
[27] Q. Yuan, Q. Liu, W.G. Song, W. Feng, W.L. Pu, L.D. Sun, Y.W. Zhang, C.H. Yan, J. Am. Chem. Soc. 139 (2007) 6698.
[28] M. Alifanti, B. Baps, N. Blangenois, J. Naud, P. Granger, B. Delmon, Chem. Mater. 15 (2003) 395.
[29] Rodriguez-Carvajal, J. Phys. B 192 (1993) 55.
[30] V.S. Escribano, E.F. Lopez, M. Panizza, C. Resini, J.M.G. Amores, G. Buscca, Solid State Sci. 5 (2003) 1369.
[31] C. Schild, A. Wokaun, R.A. Koppel, A. Baiker, J. Catal. 130 (1991) 130.
[32] M.J. Lance, J.A. Haynes, M.K. Ferber, W.R. Cannon, J. Therm. Spray Technol. 9 (2000) 68.
[33] W.H. Weber, K.C. Hass, J.R. Mcbride, Phys. Rev. B 48 (1993) 178.
[34] A. Dolbecq, J.D. Compain, P. Mialane, J. Marrot, F. Secheresse, B. Keita, L.R.B. Holzle, F. Miserque, L. Nadjo, Chem. Eur. J. 15 (2009) 733.
[35] V.I. Parvulescu, V. Parvulescu, U. Endruschat, G. Filoti, F.E. Wagner, C. Kubel, R. Richards, Chem. Eur. J. 12 (2006) 2343.
[36] S. Roy, A. Marimuthu, M.S. Hegde, G. Madras, Catal. Commun. 9 (2008) 811.
[37] C. Cattaneo, M.I.S. de Pinto, H. Mishima, B.A.L. de Mishima, D. Lescano, L. Cornaglia, J. Electroanal. Chem. 461 (1999) 32–39.
[38] M. Chatterjee, F.Y. Zhao, Y. Ikushima, Adv. Synth. Catal. 346 (2004) 459.
[39] P. Bera, K.C. Patil, V. Jayaram, G.N. Subbanna, M.S. Hegde, J. Catal. 196 (2000) 293.
[40] X. Guo, Y.Q. Sun, K. Cui, Sens. Actuators, B 31 (1996) 139.
[41] Hill Jr., An Introduction to Chemical Engineering Kinetics and Reactor Design, John Wiley Sons, New York, 1977, p. 10.
[42] K.G. Azzam, I.V. Babich, K. Seshan, L. Lefferts, J. Catal. 251 (2007) 153.
[43] K.G. Azzam, I.V. Babich, K. Seshan, L. Lefferts, J. Catal. 251 (2007) 163.
[44] P.A. Deshpande, M.S. Hegde, G. Madras, AIChE J. (2010), doi:10.1002/aic.12062.
[45] W.H. Chen, M.R. Lin, T.L. Jiang, M.H. Chen, Int. J. Hydrogen Energy 33 (2008) 6644.
[46] A. Trovarelli (Ed.), Catalysis by Ceria and Related Materials, Imperial College Press, London, 2002, p. 17.
[47] X. Liu, K. Zhau, L. Wang, B. Yang, Y. Li, J. Am. Chem. Soc. 131 (2009) 3140.
[48] T. Baidya, A. Gupta, P.A. Deshpande, G. Madras, M.S. Hegde, J. Phys. Chem. C 113 (2009) 4059.
[49] S. Roy, A. Marimuthu, M.S. Hegde, G. Madras, Appl. Catal., B 71 (2007) 23.
[50] T. Baidya, A. Marimuthu, M.S. Hegde, N. Ravishankar, G. Madras, J. Phys. Chem. C 111 (2007) 830.
[51] D. Martin, D. Duprez, J. Phys. Chem. 100 (1996) 9429.
[52] G. Jacobs, B.H. Davis, Appl. Catal., A 33 (2007) 192.
[53] J.A. Rodrigues, X. Wang, P. Liu, W. Wen, J.C. Hanson, J. Hrbek, M. Perez, J. Evance, Top. Catal. 44 (2007) 73.
[54] J.A. Rodrigues, J.C. Hanson, J.Y. Kim, G. Liu, A. Iglesias-Juez, M. Fernndez-Garca, J. Phys. Chem. B 107 (2003) 3535.
[55] G. Liu, J.A. Rodrigues, J. Hrbek, J. Dvorak, C.H.F. Peden, J. Phys. Chem. B 105 (2001) 7762.
[56] D.A. Andersson, S.I. Simak, N.V. Skorodumova, I.A. Abrikosov, B. Johanson, Appl. Phys. Lett. 90 (2007) 174119.
[57] S. Sharma, P.A. Deshpande, M.S. Hegde, G. Madras, Ind. Eng. Chem. Res. 48 (2009) 6535.
[58] G. Deganello, F. Gianicci, A. Martorana, G. Pantaleo, A. Prestinni, A. Balerna, L.F. Liotta, A. Longo, J. Phys. Chem. B 110 (2006) 8731.
[59] S. Sharma, M.S. Hegde, J. Chem. Phys. 130 (2009) 114706.
[60] K. Bakhmutsky, G. Zhou, S. Timothy, R.J. Gorte, Catal. Lett. 129 (2009) 61.
[61] J. Guzman, S. Carrettin, A. Corma, J. Am. Chem. Soc. 127 (2005) 3286.
[62] T.A. Miller, V.H. Grassian, J. Am. Chem. Soc. 117 (1995) 10969.
[63] J. Zhu, S. Albertsma, J.G. van Ommen, L. Lefferts, J. Phys. Chem. B 109 (2005) 9550.